Journal of Inflammation Research

Dovepress
open access to scientific and medical research

Open Access Full Text Article

ORIGINAL RESEARCH

Characterization of Virus Replication, Pathogenesis, and Cytokine Responses in Syrian Hamsters Inoculated with SARS-CoV-2

Shiu-Ju Yang[1]
Ting-Chun Wei[1]
Chih-Hao Hsu[1]
Sin-Ni Ho[1]
Chi-Yun Lai[2]
Shiu-Feng Huang[2,3]
Yih-Yuan Chen[4]
Shih-Jen Liu[1]
Guann-Yi Yu[1]
Horng-Yunn Dou[1,5]

[1]National Institute of Infectious Diseases and Vaccinology, National Health Research Institutes, Zhunan, Miaoli, 35053, Taiwan; [2]Pathology Core Laboratory, National Health Research Institutes, Zhunan, Miaoli, 35053, Taiwan; [3]National Institute of Molecular and Genomic Medicine, National Health Research Institutes, Zhunan, Miaoli, 35053, Taiwan; [4]Department of Biochemical Science and Technology, National Chiayi University, Chia-Yi, 60070, Taiwan; [5]Department of Biological Science & Technology, National Yang Ming Chiao Tung University, Hsinchu, Taiwan

Correspondence: Horng-Yunn Dou
National Institute of Infectious Diseases and Vaccinology, National Health Research Institutes, 35, Keyan Road, Zhunan Town, Miaoli County, 35053, Taiwan
Tel +886-37-206-166 ext 35529
Fax +886-37-583-009
Email hydou@nhri.edu.tw

Background: Severe acute respiratory syndrome coronavirus 2 (SARS-CoV-2) is a novel coronavirus which caused a global respiratory disease pandemic beginning in December 2019. Understanding the pathogenesis of infection and the immune responses in a SARS-CoV-2-infected animal model is urgently needed for vaccine development.

Methods: Syrian hamsters (*Mesocricetus auratus*) were intranasally inoculated with 10^5, 5×10^5, and 10^6 $TCID_{50}$ of SARS-CoV-2 per animal and studied for up to 14 days. Body weight, viral load and real-time PCR amplification of the SARS-CoV-2 *N* gene were measured. On days 3, 6 and 9, lung, blood, liver, pancreas, heart, kidney, and bone marrow were harvested and processed for pathology, viral load, and cytokine expression.

Results: Body weight loss, increased viral load, immune cell infiltration, upregulated cytokine expression, viral RNA, SARS-CoV-2 nucleoprotein, and mucus were detected in the lungs, particularly on day 3 post-infection. Extremely high expression of the pro-inflammatory cytokines MIP-1 and RANTES was detected in lung tissue, as was high expression of IL-1β, IL-6, IL-12, and PD-L1. The glutamic oxalacetic transaminase/glutamic pyruvic transaminase (GOT/GPT) ratio in blood was significantly increased at 6 days post-infection, and plasma amylase and lipase levels were also elevated in infected hamsters.

Conclusion: Our results provide new information on immunological cytokines and biological parameters related to the pathogenesis and immune response profile in the Syrian hamster model of SARS-CoV-2 infection.

Keywords: SARS-CoV-2, hamster, immune response, pathogenesis

Introduction

Coronavirus disease 2019 (COVID-19) is caused by a new coronavirus, SARS-CoV -2, which produced a pandemic of severe pneumonia worldwide beginning in December 2019.[1] SARS-CoV-2 was identified in atypical pneumonia patients who had visited the Huanan seafood market in Wuhan, China. Till today, SARS-CoV-2 spread quickly to 223 countries worldwide, and has caused more than 3.954 million deaths.[2] The number of deaths and confirmed cases are still climbing. To help combat COVID-19 and future coronavirus outbreaks, an easy-to-handle small animal model for the development of vaccines and therapies is urgently needed.

The amino acid sequence of angiotensin-converting enzyme 2 (ACE2) of the Syrian hamster (*Mesocricetus auratus*) is highly homologous to that of humans (hACE2), the cell receptor for both SARS-CoV[3] and SARS-CoV-2.[4] This makes

Received: 4 June 2021
Accepted: 1 August 2021
Published: 11 August 2021

the Syrian hamster a particularly attractive animal model for SARS-CoV[5,6] and SARS-CoV-2 infection.[4,7–11] Following infection with SARS-CoV-2, Syrian hamsters display respiratory signs, lose weight and recover spontaneously over 14 days,[4,8] similar to a mild course of COVID-19 in humans. Moreover, multiple labs have reported information about the pathology, clinical manifestations, and some transmission routes in Syrian hamsters.[4,7–13] An alternative small animal model utilizes human ACE2 transgenic mice,[12,13] which when infected with SARS-CoV-2 become moribund, mirroring the clinical expression of severe COVID-19 patients. However, transgenic hACE2 mice are proprietary, and establishing new lines is both time-consuming and labor-intensive. More importantly, unlike hACE2 mice, up to 56% of SARS-CoV-2-infected individuals are asymptomatic even at hospital admission.[14] These observations suggest that the hamster model may be the best currently available option.

Fortunately, most scientists are optimistic about the efficacy of several new anti-SARS-CoV-2 vaccines such as those developed by Pfizer-BioNTech, Moderna, AstraZeneca and Johnson & Johnson. However, there is no guarantee that these vaccines will be effective and afford long-term protection against all SARS-CoV-2 variants. For this reason, it is important to know the pathogenesis, immune responses and hematology of SARS-CoV-2 infection in the hamster model. Here, we report detailed information about the histopathology, immunological cytokine profile, and blood biological analysis in SARS-CoV-2-infected Syrian hamsters, and compare the clinical signs and disease evolution between humans and the hamster model.

We detected high levels of virus, viral RNA and nucleoprotein expression in SARS-CoV-2-infected hamster lung at 3 days post-infection (d.p.i) by $TCID_{50}$, quantitative PCR (qPCR), in situ hybridization, and immunohistochemistry (IHC) assays. Lung infiltration by neutrophils, macrophages, and lymphocytes was prominent, as were hyaline membrane formation and edema. Elevated secretion of pulmonary mucus was also observed. Upregulation of the pro-inflammatory cytokines MIP-1 and RANTES was detected at 3 d.p.i., while the immune suppressor genes IL-10 and PD-L1 were also upregulated. Blood biological and chemistry results showed that amylase, lipase levels and the glutamic oxalacetic transaminase/glutamic pyruvic transaminase (GOT/GPT) ratio were all increased in the infected group. High viral copy numbers were detected in the liver and pancreas as well. Understanding the pathogenesis of SARS-CoV-2 and the immune responses to the virus in hamsters will aid in the development of therapies for humans.

Materials and Methods

Virus

Beta CoV/SARS-CoV-2/Taiwan/2020-004 was isolated from a confirmed COVID-19 patient originally from Wuhan (China) on March 2020 in Taiwan. The virus was amplified and a viral bank was produced in Vero E6 cells at the BSL-3 facility, National Health Research Institutes (NHRI). Stock virus (2.29×10^7 $TCID_{50}$/mL) was prepared after 2–3 passages in Vero E6 cells in Dulbecco's Modified Eagle's Medium (DMEM) with 4.5 g/L glucose, 100 mg/L sodium pyruvate, 10% fetal bovine serum (FBS), 100 μg/mL penicillin-streptomycin. For determining the viral load of infected animals, viral titers of the supernatant were measured using a standard 50% tissue culture infection dose ($TCID_{50}$) assay.

Animal Experiments

Male Syrian hamsters (*Mesocricetus auratus*) aged 6 to 8 weeks were purchased from the National Laboratory Animal Center (Taipei, Taiwan). All hamsters were randomized into groups and kept in individually ventilated cage environments at the Animal Center of the NHRI and then transferred to an ABSL3 facility, NHRI (Maoli, Taiwan). Animal experiments were reviewed and approved by the NHRI Institutional Animal Care and Use Committee. We conducted experiments according to guidelines set out by the Association for Assessment and Accreditation of Laboratory Animal Care International (AAALAC, NHRI, Taiwan). Two sets of experiments were conducted. In the first, hamsters were infected with 10^5, 5×10^5, and 10^6 $TCID_{50}$ of SARS-CoV-2 in 50 μL PBS per hamster (n=5 per group) on day 0 by intranasal inoculation after inhalation of isoflurane. Body weight and clinical signs of infected animals were monitored closely daily for 14 days. Blood, lungs, and trachea were collected on day 3 and day 14. Half of each organ was used to determine viral load ($TCID_{50}$) and genome amount (qPCR). The other half of each organ was fixed in 4% formalin for pathologic examination. In the second set of experiments, hamsters were infected with 5×10^5 $TCID_{50}$ of SARS-CoV-2 in 50 μL PBS per hamster on day 0 by intranasal inoculation. Animals were sacrificed on days 3,

6, and 9 post-infection (n=5 per group), without perfusion. Blood, lungs, trachea, liver, pancreas, heart, and kidneys were collected. As in the first set, half of each organ was used to determine the viral load ($TCID_{50}$) and genome amount (qPCR), and the other half was fixed in 4% formalin for pathologic examination and immunohistochemical staining.

In situ Hybridization

Samples of lung tissue were fixed in formalin and embedded in paraffin using routine methods. RNA probe synthesis (anti-SARS-CoV-2 nucleoprotein gene, 500 bp) followed the protocol of the Roche DIG RNA labeling kit (Sigma-Aldrich, Roche, Mannheim, Germany). The in situ hybridization reaction was performed by following the protocol of the DIG application manual (4^{th} edition). Briefly, the sections were hybridized with 20 μg/mL of RNA probe and incubated at 55°C for 16 hours. Alkaline phosphatase-labeled anti-DIG antibody (1:2500) was applied and incubated for 1 hour. Finally, the sections were colored with NBT/BCIP cocktail for 16 hours and counterstained with methyl-green.

Periodic Acid Schiff's Stain (PAS), Immunohistochemical Staining (IHC) and Pathologic Score

Samples of lung tissue were fixed in formalin and embedded in paraffin using routine methods, and the sections were then stained with hematoxylin and eosin (H&E). Tissue processing was performed by the core pathology facility at the NHRI (Maoli, Taiwan). Histopathologic parameters (ie, peribronchiolitis, perivasculitis, alveolitis), lesion frequency and severity were incorporated into all pathologic examinations. For PAS staining, paraffin sections were rehydrated and processed following the PAS staining protocol (BioVision, Milpitas, CA, USA). For IHC, paraffin sections were rehydrated and the antigens retrieved with 10 mM citrate buffer (pH 6.0) at 100°C for 5 min. After blocking the peroxidase activity and background (IHC/ICC kit, BioVision, Milpitas, CA, USA), the serial sections were incubated with primary antibody anti-SARS-CoV nucleoprotein (Sino Biological, cat. No. 40143-T62, PA, USA) and stained following the manufacturer's protocol (BioVision). Finally, the sections were colored with the chromogen DAB and counterstained with hematoxylin.

Detection of COVID-19 Anti-Spike Neutralizing Antibody

Hamster plasma was collected at 3, 6, and 9 d.p.i by using EDTA as an anticoagulant and stored at −80°C until use. Diluted plasma was assayed by following the protocol of the neutralizing antibody ELISA kit (Abnova, Zhongli, Taiwan). Briefly, human ACE2 protein was coated on plates at 4°C overnight. Then, diluted plasma samples and COVID-19 spike RBD rabbit Fc-tag protein were co-incubated for 2 hours. After washing, HRP-conjugated goat anti-rabbit antibody was added and incubated for 1 hour. Finally, TMB reagent was applied to initiate the color reaction and stopped after 5 min. A standard curve was determined by positive control antibody, which was diluted from 250 ng/mL. The plate was read at an absorbance of 450 nm with an ELISA plate reader (Bio-Rad, iMark, CA, USA).

RNA Extraction and Quantitative PCR

Total RNA was extracted by Trizol reagent or AVL buffer (Qiagen, QIAmp Viral RNA extraction kit), and cDNA was prepared by using a reverse transcription kit (ThermoFisher Scientific, CA, USA). Viral RNA qPCR was determined by using a KAPA probe fast universal One-step qRT-PCR kit (KAPA Biosystems, USA). Primer sequences are shown in Table 1. The mRNA levels of IL-1β, IL-4, IL-10, IL-12, IL-17, IFN-γ, iNOS, MCP-1, MIP-1, PD-L1, RANTES, TGF-β, and TNF-α, various transcription factors and GAPDH were detected by real-time quantitative PCR analysis using the ABI QuantStudio 6 Flex system (Applied Biosystems, Foster City, CA, USA). Cytokine and GAPDH levels were calculated relative to amounts found in a standard sample, and cytokine levels were corrected for GAPDH mRNA levels to normalize for RNA input. Relative expression (Relative index) is presented as $2^{-\Delta\Delta CT}$.

Blood Test for Biology and Chemistry Analysis

Hamster plasma was assayed by using Fuji Dri-Chem slides (Fujifilm Dri-Chem 4000, Tokyo, Japan) following the manufacturer's protocol.

Multi-Plex Immunoassay

Cytokine and chemokine expression levels in plasma were detected with a Multi-Plex immunoassay by the Inflammation Core Facility (Institute of Biomedical Sciences, Academia Sinica, Taipei, Taiwan).

Table 1 Primer Sequences for qPCR of Hamster Gene Expression

Primer Name	Sequence (5′-3′)		Accession Number
GADPH	Forward Reverse	TCATCAATGGGAAGGCCAACA AAGGTGTGGAGATGATGACCC	XM_013124485.3
IFN-γ	Forward Reverse	GCATCTTGGCTTTGTTGCTC GATCTGGCTCTCAATGATTTTTGT	NM_001281631.1
IL-10	Forward Reverse	TGGGAAACCTCGTTGTACCT AATACTACCACGCGTCCCT	XM_005079860.3
IL-4	Forward Reverse	TCCACGGAGAAAGACCTCATC GGACTCATTCACATTGCAGCTC	XM_005067769.3
iNOS	Forward Reverse	TGGCAGGATGGGAAACTGA GCACCGCTTTCACCAAGACT	AY297461.1
IL-12p35	Forward Reverse	GGCCTTCCCTGGCAGAA ATGCTGAAAGCCTGCAGTAGAAT	AB085791.1
IL-1β	Forward Reverse	TGATGCTCCCATTCGACAGC TTCTTTCCCTTTAGGCCCAGG	AB028497
IL-6	Forward Reverse	CAACCCTGGCTGTATGGACA GTGCTCTGAATGACTCTGGCT	AB028635.1
IL-17a	Forward Reverse	TCCAAACACTGAGGCCAAGAA ACAGAGTTCATGTGGTGGTCC	XM_005072283
TGF-β	Forward Reverse	CCAATGCCACCACAGGAGAT TTGGGTTGAGTGACCACCAC	XM_005065875
TNF-α	Forward Reverse	CTGAACTTCGGGGTGATCGG TGAGAGACATGCCGTTGGC	AF046215.1
RANTES	Forward Reverse	CTCTACGCTCCTTCATCTGCC CTTTGGGTTGGCACACACTTG	XM_005076936
PD-L1(CD274)	Forward Reverse	CGGCTCCCAAGGAACTGTATG GAAGCTGCTGTGTTGATGCTT	XM_005063709
MIP-1α	Forward Reverse	TGGTGCTGACACCCTAACCT GGTCAGCGACGTACTCTTGG	NM_001281338
MCP-1	Forward Reverse	TCCTGCAAGTCAATCCTGCC GAAGTGATGGAGAGACGGGC	AY007988.1

Statistical Analysis

All results are presented as mean ± SEM for three to five hamsters per group. The statistical significance between the two experimental groups was assessed using a two-tailed unpaired Student's *t*-test. While analyzing multiple groups, one-way analysis of variance (ANOVA) with a Tukey post-hoc test was applied for comparisons involving one independent variable; and two-way ANOVA with a Bonferroni post-hoc test was applied for comparisons involving two variables. The differences were considered significant for *P* values less than 0.05. Statistical tests were performed using GraphPad Prism version 5.0 (GraphPad Software, La Jolla, CA, USA).

Results

Physiological Parameters and Viral Load in Syrian Hamsters Infected with Different Challenge Doses of SARS-CoV-2

Male Syrian hamsters (6–8 weeks old, n=5 per group per time point) were infected intranasally with 10^5, 5×10^5 and

10^6 $TCID_{50}$ of SARS-CoV-2 on day 0 and monitored for 14 days. Body weight, breathing, physical signs and survival were measured daily for 14 days. After the infection, the animals showed fatigue, lethargy, ruffled fur, and hunched back. Body weight of the infected animals decreased, becoming significantly different from that of the control animals by day 3, and continuing to decline until day 6, at which point the weight loss was about 10%; subsequently, body weight slowly increased each day until day 14 (Figure 1A). All three infection doses produced the same pattern of weight loss and recovery, with no significant difference among them (Figure 1A). No infected or control animals died during the 14 days. Five hamsters from each group were sacrificed on day 3, and the viral load ($TCID_{50}$ of infection dose of $10^5 = 2.958 \pm 1.217x10^8$, infection dose of $5\times10^5 = 3.57 \pm 0.608x10^8$, infection dose of $10^6 = 7.226 \pm 1.818\times10^8$) and SARS-CoV-2 *N* gene copy number (qPCR, infection dose of $10^5 = 6.333 \pm 3.123x10^6$, infection dose of $5\times10^5 = 3.179 \pm 0.493x10^6$, infection dose of $10^6 = 2.210 \pm 0.277\times10^6$) in the lungs were determined. For each infection dose, the viral load was found to be about 10^8 $TCID_{50}$ per lung (Figure 1B); the $TCID_{50}$ of the non-infected control group was zero. The number of copies of the SARS-CoV-2 *N* gene was estimated to be 10^6–10^7/μg RNA for all three doses of virus (Figure 1C). The patterns for the viral load and SARS-CoV-2 *N* gene results are consistent.

Pathology, SARS-CoV-2 Nucleoprotein IHC, and PAS Staining of the Lungs

On day 3 and 14 post-infection, hamster lungs were processed for H&E staining, IHC, and periodic acid Schiff's (PAS) staining. Inflammation of the lungs was notable, revealed as a patchy, bronchopneumonia pattern. On day 3, several foci of inflammatory cell infiltration, with predominantly mononuclear cells, neutrophils and some macrophages, were observed (Figure 1 D, 3 d.p.i, yellow dotted circle). These involved the alveolar septa and air spaces, which were filled by cells to variable extents (Figure 1D). Mild fluid and focal, thin fibrin could also be found. The bronchioles of the affected areas exhibited intraluminal

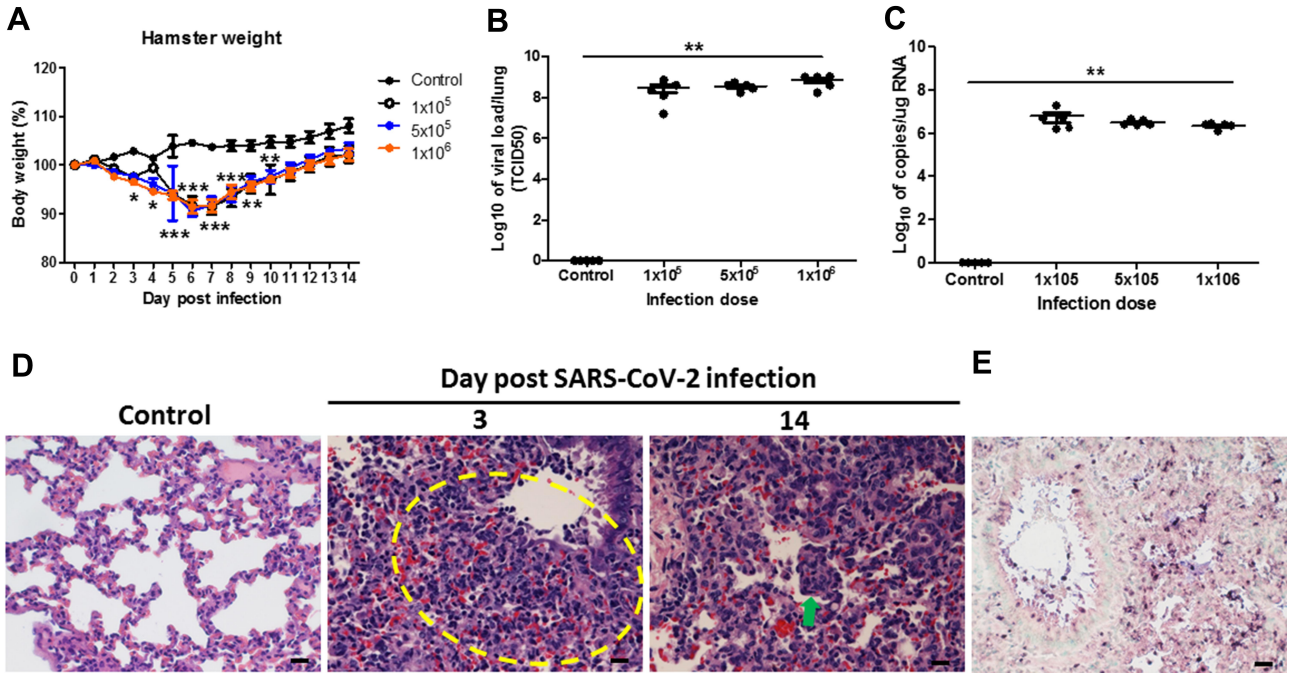

Figure 1 Body weight change, viral load, and pathological changes of SARS-CoV-2-infected Syrian hamsters following different challenge doses. (**A**) Body weights of hamsters infected with 10^5, 5×10^5, and 10^6 $TCID_{50}$ of SARS-CoV-2 (n=5 per group, and non-infected control, n=5) over 14 days (compared with the weight on day 0). Differences among groups were determined using two-way ANOVA with a Bonferroni post hoc test (*P<0.05; **P < 0.01; ***P < 0.001, control vs all infected groups). (**B**) Viral loads ($TCID_{50}$/lung) of hamsters infected with 10^5, 5×10^5, and 10^6 $TCID_{50}$ of SARS-CoV-2 (n=5 per group, and non-infected control, n=5) on day 3. Differences among groups were determined using one-way ANOVA with a Tukey post hoc test (**P < 0.01, control vs 10^6). (**C**) Quantitative PCR of the SARS-CoV-2 *N* gene in hamsters infected with 10^5, 5×10^5, and 10^6 $TCID_{50}$ of SARS-CoV-2 on day 3. Differences among groups were determined by using one-way ANOVA with a Tukey post hoc test (**P < 0.01, control vs 10^6). (**D**) On days 3 and 14, samples of lung tissue were fixed in formalin and embedded in paraffin using routine methods, and the sections were then stained with H&E. Yellow dotted circle outlines several foci of inflammatory cell infiltration, with predominantly mononuclear cells, neutrophils and some macrophages. Green arrow presents macrophage aggregates in the airway and alveolar spaces. The panels show representative results from the 5×10^5 $TCID_{50}$ infection dose. Scale bar for 400× panels = 20 μm. (**E**) In situ hybridization. The sections were hybridized with *N* gene RNA probe (anti-nucleoprotein). The panels show representative results from the 5×10^5 $TCID_{50}$ infection dose. Scale bar for 200× panels = 50 μm.

secretions, macrophages, and variable amounts of inflammatory cell exudate. Heavy interstitial lymphocytic infiltration mixed with some neutrophils was present in the lung parenchyma at 3 d.p.i., which is consistent with acute pneumonia. At 14 d.p.i., the inflammatory foci persisted, while the numbers of neutrophils and mononuclear cells were decreased. There was thickening of the alveolar septa, with alveolar cell hyperplasia, bronchiolization, increased numbers of fibroblasts, and presence of macrophage aggregates (Figure 1D). A fibroblast plug was also found in some cases, suggestive of an organizing phase of pneumonia. The interstitial inflammatory cell infiltration was markedly decreased. Instead, there was thickening of the alveolar septa, with alveolar cell hyperplasia, and presence of macrophage aggregates in the airway and alveolar spaces (Figures 1D, 14 d.p.i., green arrow). The above features are consistent with a convalescent stage of pneumonia. The pneumonia pattern present the same signs in all of three infectious doses, no difference among them. No cell infiltration or inflammation was evident in the trachea, heart and kidney at 14 d.p.i. (Supplementary Figure 1).

We also synthesized an RNA probe (complementary to the viral *N* gene sequence) to hybridize with SARS-CoV-2 viral RNA. At 3 d.p.i., viral RNA was detected in the consolidation of pneumocytes, neutrophils and macrophages, and some even appeared in the mucus secreted into the bronchiolar space (Figure 1E). Next, we detected the expression of SARS-CoV-2 nucleoprotein (the product of *N* gene) in the lungs by IHC. All three infection doses elicited high expression of nucleoprotein at 3 d.p.i. (Figure 2A), which was not observed in non-infected control lung tissue.

Severe COVID-19 patients secrete large amounts of mucus. To examine this feature in hamsters, we performed PAS staining of lung tissue to stain polysaccharide, which

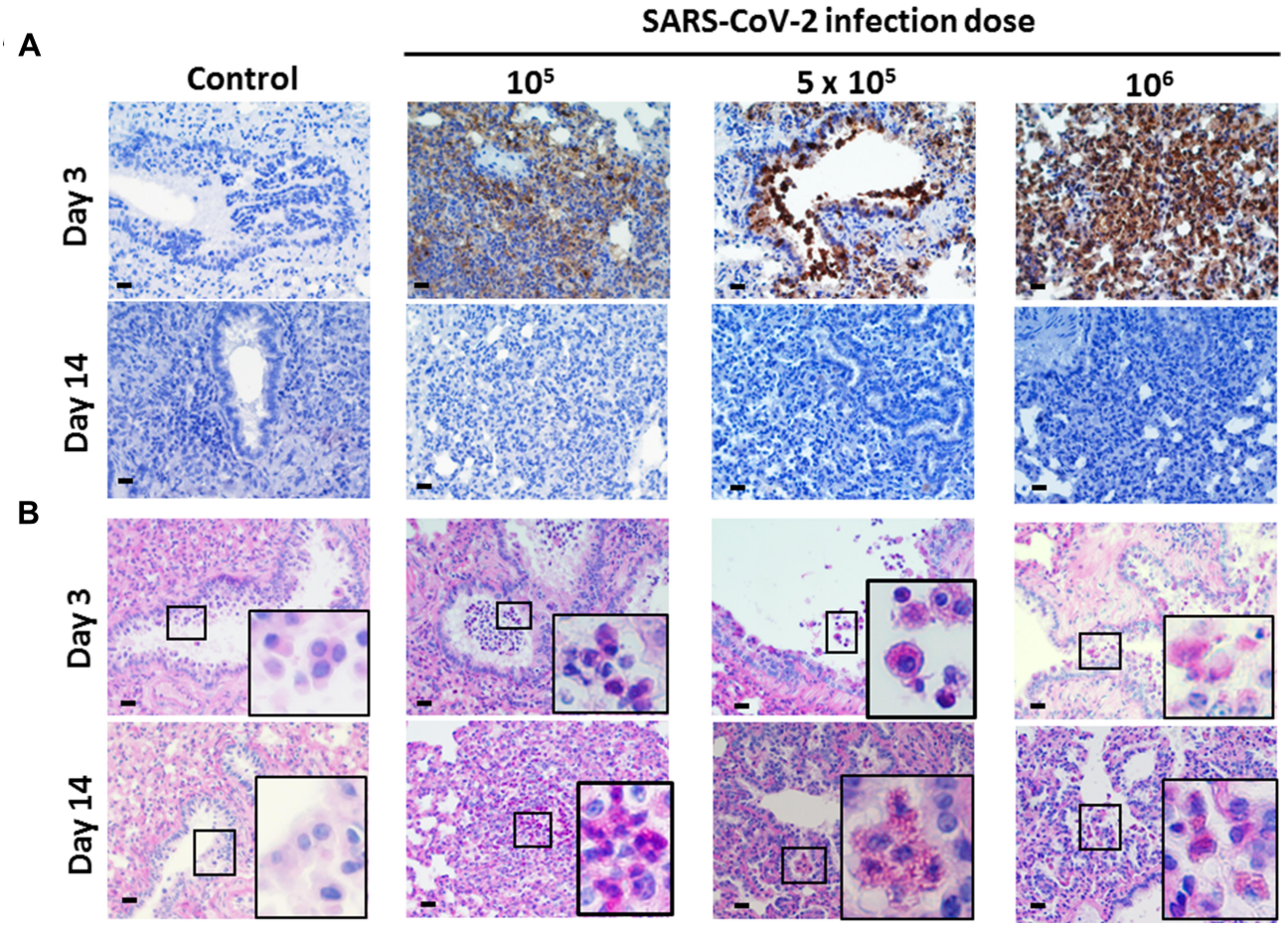

Figure 2 SARS-CoV-2 nucleoprotein expression and mucosal mucus levels in SARS-CoV-2-infected Syrian hamsters following different challenge doses. Hamsters aged 6 to 8 weeks (n=5) were infected with 10^5, 5×10^5, and 10^6 $TCID_{50}$ of SARS-CoV-2 on day 0. (**A**) On days 3 and 14, samples of lung tissue were dissected, fixed in formalin and embedded in paraffin using routine methods, and the sections were then stained with anti-SARS-CoV nucleoprotein antibody. (**B**) PAS staining was performed on the same paraffin-embedded sections. The small box frame in each panel shows the macrophages that scavenged the extra mucus near the trachea. The large box frame shows an enlargement of macrophage phagocytosis. Scale bar for the 100× panels = 200 μm, for the 400× panels = 20 μm.

is the main component of mucus. All macrophages in non-infected control lung showed a clear cytosol background, whereas the macrophages and phagocytes in infected lung tissue, having phagocytized extra mucus and debris, were stained red (Figure 2B, day 3 and day 14). These results show that SARS-CoV-2 caused elevated secretion of mucus within the lungs and bronchioles.

Dynamic Changes of Viral Load and SARS-CoV-2 Nucleoprotein Expression in the Lungs and Extrapulmonary Organs

To investigate dynamic changes of viral load and pathology during SARS-CoV-2 infection, Syrian hamsters (6–8 weeks old; n=5 per infected group, and n=3 for the non-infected control) were infected intranasally with 5×10^5 $TCID_{50}$ of virus on day 0 and then sacrificed at 3, 6, and 9 d.p.i. Blood, lung, liver, pancreas, heart, kidney, peripheral blood mononuclear cells (PBMC), and bone marrow (BM) were harvested for further study. The viral load of the lungs was highest at 3 d.p.i., declined by day 6 (Figure 3A) and reached a value of zero at 9 d.p.i. (Figure 3A). The same lung samples were also tested for the SARS-CoV-2 *N* gene by qPCR. The viral copy number in the lung was highest at 3 d.p.i. (approx. 10^6 copies/μg RNA), dropped to 10^5 copies/μg RNA at 6 d.p.i., and was still present at 10^2 copies/μg RNA at 9 d.p.i. (Figure 3B). In contrast, extrapulmonary organs showed different patterns: in liver, the viral copy number were about 10^4 copies/μg RNA at 3 d.p.i., the number increased to 10^5 copies/μg RNA at 6 d.p.i. (Figure 3C). In pancreas, the viral copy number were 10^4 copies/μg RNA at 3 d.p.i., and kept the same level at 6 d.p.i. (Figure 3D). This suggests that the virus attacked the liver and pancreas. In heart, kidney, PBMC, and BM, the viral copy numbers were about 10–10^2 copies/μg RNA (Figure 3E–H). This means that viral spreading and replication beyond the lungs occurred at low levels over the 9-day study period.

Dynamic Changes of Pathology, SARS-CoV-2 Nucleoprotein Expression and PAS Staining in Lung and Extrapulmonary Organs

At 3 d.p.i., hamsters inoculated with 5×10^5 $TCID_{50}$ of SARS-CoV-2 showed heavy lymphocytic infiltration in the lung parenchyma, with some neutrophils in the alveolar spaces, which is consistent with acute pneumonia. At 6 d.p.i., the interstitial inflammation had progressed, with involvement of most lung parenchyma. Hyaline membrane formation was also found (Figures 4A and 6 d.p.i., blue

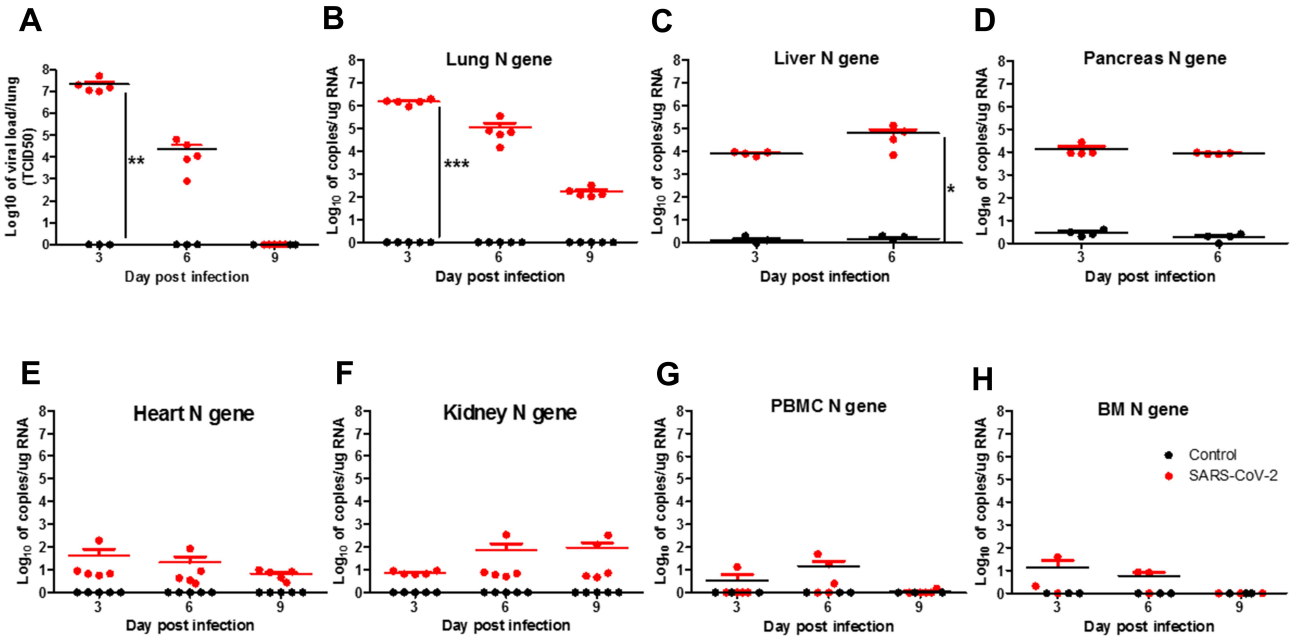

Figure 3 Viral load changes and tissue tropism in SARS-CoV-2-infected Syrian hamsters on days 3, 6, and 9 post-infection. (**A**) Viral loads ($TCID_{50}$/lung) of hamsters infected with 5×10^5 $TCID_{50}$ of SARS-CoV-2 (n=5 for SARS-CoV-2, and n=3 for non-infected controls) on days 3, 6, and 9 (**B, E–H**). N=4 for panel (**C** and **D**). Quantitative PCR of hamster lung (**B**), liver (**C**), pancreas (**D**), heart (**E**), kidney (**F**), PBMC (**G**), and bone marrow (BM) (**H**) of the SARS-CoV-2 *N* gene (from CCDC) on days 3, 6, and 9 post-infection. Differences among groups were determined using two-way ANOVA with a Bonferroni post hoc test (*P<0.05, control vs SARS-CoV-2 at 6 d.p.i.; **P < 0.01, control vs SARS-CoV-2 at 3 d.p.i.; ***P < 0.001, control vs SARS-Cov-2 at 3 d.p.i.) in panels (**A–H**), p value is not shown for no significance among groups.

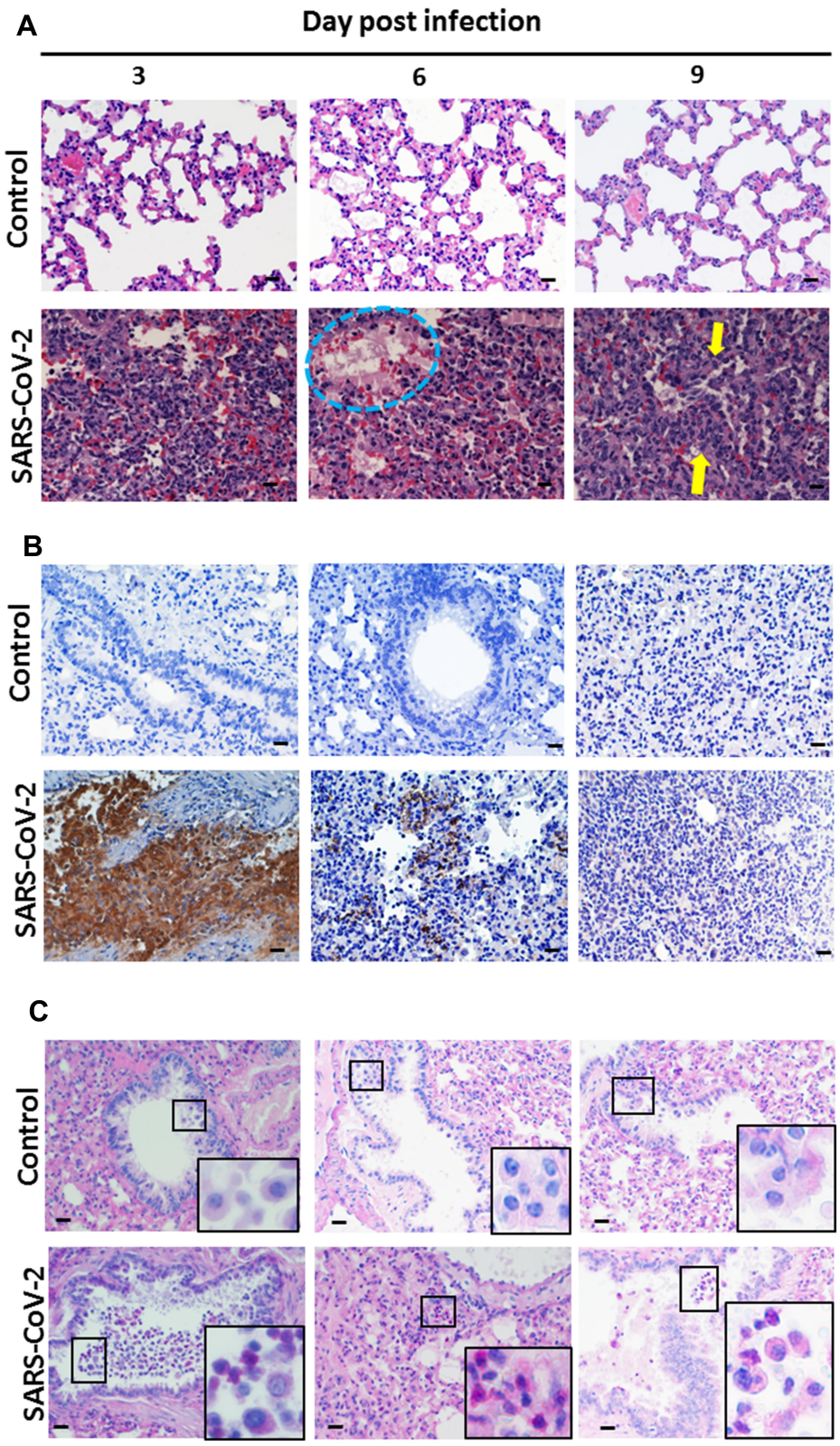

Figure 4 Pathological changes in SARS-CoV-2-infected hamster lung on days 3, 6, and 9 post-infection. Syrian hamsters aged 6 to 8 weeks (n=5 for SARS-CoV-2, and n=3 for non-infected control) were infected with 5×10^5 $TCID_{50}$ of SARS-CoV-2 on day 0. On days 3, 6, and 9, samples of lung and trachea tissue were removed, fixed in formalin and embedded in paraffin using routine methods, and then processed for staining. (**A**) Samples of lung sections stained with H&E. The blue dotted circle outlines hyaline membrane formation. The yellow arrows present macrophage aggregates in the airway and alveolar spaces. (**B**) Lung sections immunostained with anti-SARS-CoV nucleoprotein antibody. (**C**) PAS staining showing mucus expression in hamster lung. Small box frames show macrophages that scavenged the extra mucus near the trachea. Large box frames show enlargements of macrophage phagocytosis. Scale bar for the 400× panels = 20 μm.

dotted circle), which is consistent with diffuse alveolar damage. At 9 d.p.i., the interstitial inflammatory cell infiltration was decreased, but there was prominent alveolar cell hyperplasia and presence of macrophage aggregates in the airway and alveolar spaces (Figure 4A, yellow arrow). The severity of the septal edema, the number of inflammatory cells, and the nucleomegaly had all diminished. Fibrin was no longer detected. Thus, the pneumonia had begun to resolve after 6 d.p.i. (Figure 4A). All pathological findings are summarized in Table 2.

We also performed IHC for detection of SARS-CoV-2 nucleoprotein in the lungs, liver, pancreas, heart, and kidneys. Extensive expression of SARS-CoV-2 nucleoprotein was detected in the lungs at 3 d.p.i. (control lung tissue was perfectly clear) (Figure 4B). At 6 d.p.i., the expression of SARS-CoV-2 nucleoprotein was dramatically decreased, even though signs of inflammation filled the alveolar space; at 9 d.p.i., the expression of SARS-CoV-2 nucleoprotein in the lungs was barely detectable (Figure 4B). This suggests that the infiltrating immune cells were highly effective in clearing the virus after 3 d.p.i.

The results of PAS staining of lung sections showed that macrophages near the bronchioles had scavenged (phagocytized) cell debris, mucus, and presumably pathogens, as they were stained red (Figure 4C). All of the macrophages in non-infected control lungs showed clear cytosolic backgrounds (Figure 4C). This suggests that SARS-CoV-2 caused the secretion of significant amounts of intrabronchiolar mucus.

Table 2 Histopathologic Characterization of SARS-CoV-2-Infected (5×10^5 $TCID_{50}$) Hamster Lung

Pathological Finding	-: No Observation, +: Mild, ++: Severe
Edema	+
Consolidation (pneumonia and bronchopneumonia)	+
Alveolar hemorrhage	+
Diffuse exudative alveolar injury	++
Alveolar hyaline membrane	+
Inflammation	+
Necrosis and septal destruction	-
Pneumocyte shedding	+
Eosinophilic inclusion in pneumocytes	-
Pneumocyte transformation to multinucleated giant cells	+
Alveolar epithelial hyperplasia	++
Alveolar wall thickening and extracellular matrix deposition	+
Neutrophilic capillaritis	-
Pulmonary fibrosis	-

No inflammation and cell infiltration appeared in the SARS-CoV-2-infected liver (Figure 5A); however, irregular arrangement of structure, more numerous and larger vacuoles in the cytosol, enlarged cells, and more duplicated (polyploid) nuclei in hepatocytes appeared in the infected organ at 3 d.p.i. and 6 d.p.i. (Figure 5A), compared with the normal control liver. Both at 3 and 6 d.p.i., expression of SARS-CoV nucleoprotein was detected in the hepatocytes, and the DAB-stained larger vacuoles forced the nucleus to one side (Figure 5B); the control liver showed no nucleoprotein expression. These results show the viral infection caused histologic abnormalities and viral replication in the liver.

No apparent acute pancreatitis, cardiovascular abnormalities or acute renal failure (or acute kidney injury) were evident by H&E staining of pancreas, heart and kidney (Figure 5A). Nor was SARS-CoV-2 nucleoprotein expression detected in sections of these organs at 3 d.p.i. and 6 d.p.i. (Figure 5B). Thus, the few viruses detected in these organs by qPCR assay (Figure 3D–F) did not generate overt inflammation or tissue damage.

Dynamic Changes of Anti-Spike Antibody with Neutralizing Potential in SARS-CoV-2–Infected Plasma

It is important to know whether Syrian hamsters generate neutralizing antibody that interferes with binding of SARS-CoV-2 to hACE2 on the surface of human cells. To detect whether hamsters generate antibody with neutralizing potential, plasma from control and SARS-CoV-2-infected hamsters was tested for reactivity to the viral spike protein's receptor-binding domain, which recognizes and binds hACE2. At 3 d.p.i., anti-spike antibody was not detected in the plasma of hamsters infected with 10^5, 5×10^5, and 10^6 $TCID_{50}$ (Figure 6A, compared with control hamsters); all antibody values are similar to those of the negative control. However, at 6 d.p.i., two of five hamsters infected with 5×10^5 $TCID_{50}$ showed presence of anti-spike antibody (Figures 6B, 49.597 μg/mL and 69.993 μg/mL, respectively). At 9 d.p.i., all five hamsters expressed anti-spike antibody (Figure 6B, anti-spike Ab = 87.448 ± 11.96 μg/mL), compared with the control at 9 d.p.i. (Figure 6B, anti-spike Ab = 11.805 ± 7.245 μg/mL, $***P<0.001$, compared with control). These results indicate that antibodies with neutralizing potential are generated by 6 d.p.i. and continue to increase through 9 d.p.i.

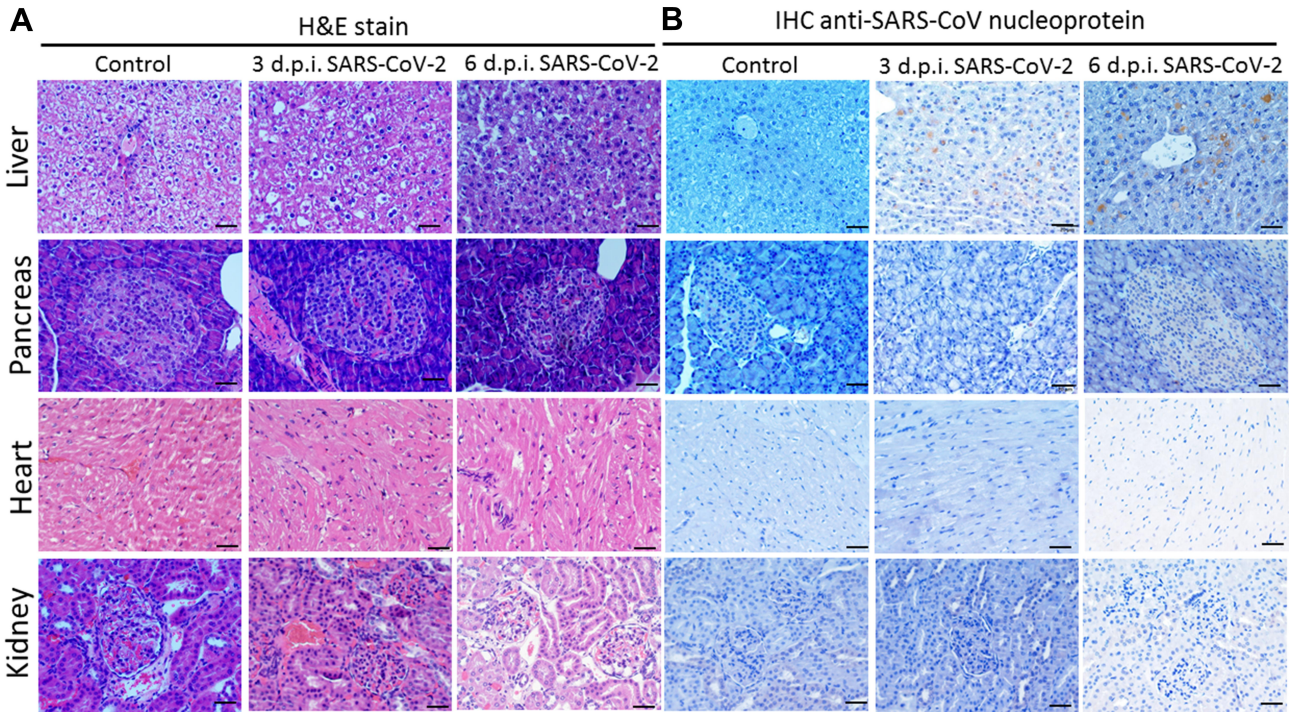

Figure 5 SARS-CoV nucleoprotein expression in SARS-CoV-2-infected hamsters post-infection day 3 and 6. (**A**) Syrian hamsters aged 6 to 8 weeks (n=5 for SARS-CoV-2, and n=3 for non-infected control) were infected with 5×10^5 $TCID_{50}$ of SARS-CoV-2. Liver, pancreas, heart and kidney sections were stained by H&E on day 3 and 6. (**B**) IHC staining for SARS-CoV nucleoprotein expression in the tissue sections. Scale bar for 400× panels = 20 μm.

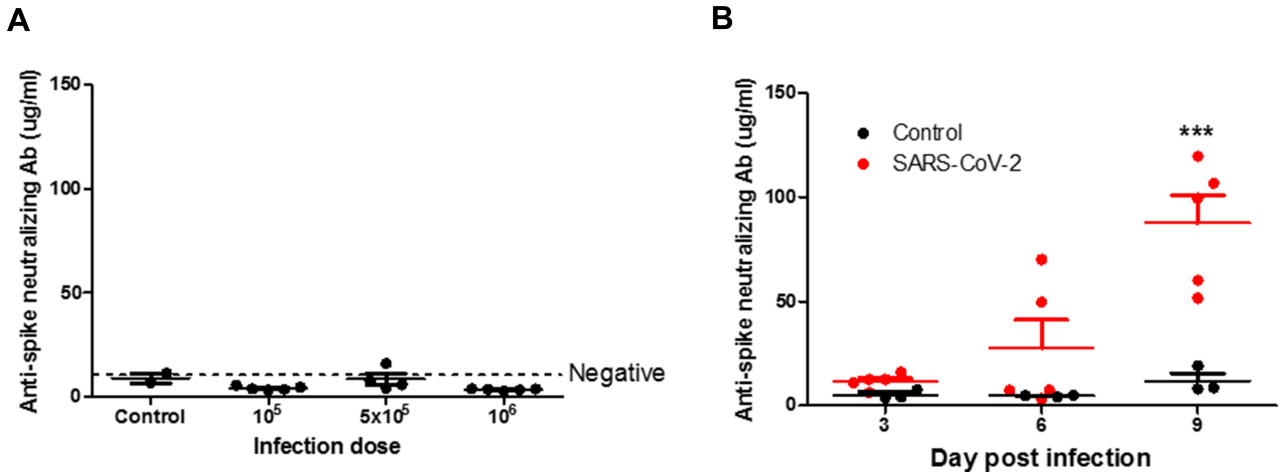

Figure 6 Anti-spike neutralizing antibody in SARS-CoV-2-infected hamsters. (**A**) Syrian hamsters aged 6 to 8 weeks (n=5 for SARS-CoV-2, and n=3 for non-infected control) were infected with 10^5, 5×10^5, and 10^6 $TCID_{50}$ of SARS-CoV-2 on day 0. Anti-spike neutralizing antibody of plasma was detected by ELISA following the manufacturer's protocol. Differences among groups were determined using one-way ANOVA with a Tukey post hoc test, $P>0.05$, no significant among all groups. (**B**) Syrian hamsters aged 6 to 8 weeks (n=5 for SARS-CoV-2, and n=3 for non-infected control) were infected with 5×10^5 $TCID_{50}$ of SARS-CoV-2 on days 3, 6, and 9. Anti-spike neutralizing antibody of plasma was detected by ELISA following the manufacturer's protocol. Differences among groups were determined using two-way ANOVA with a Bonferroni post hoc test (***$P < 0.001$, control vs SARS-CoV-2 at 9 d.p.i.).

High Expression of IL-1β, IL-6, IL-10, IL-12, IFN-γ, MIP-1α, PD-L1, and RANTES in SARS-CoV-2-Infected Lung

Some clinical studies have reported the appearance of cytokine storms in COVID-19 patients, which caused their death.[15,16] Due to limited detection tools for hamster biomolecules, we designed multiple primers to measure cytokine expression by qPCR. Primer sequences are shown in Table 1. We detected upregulation of numerous inflammatory cytokines in the lungs of SARS-CoV -2-infected Syrian hamsters, including IL-1β (Figure 7A), IL-6 (Figure 7C), IL-12 (Figure 7E), IFN-γ (Figure 7G),

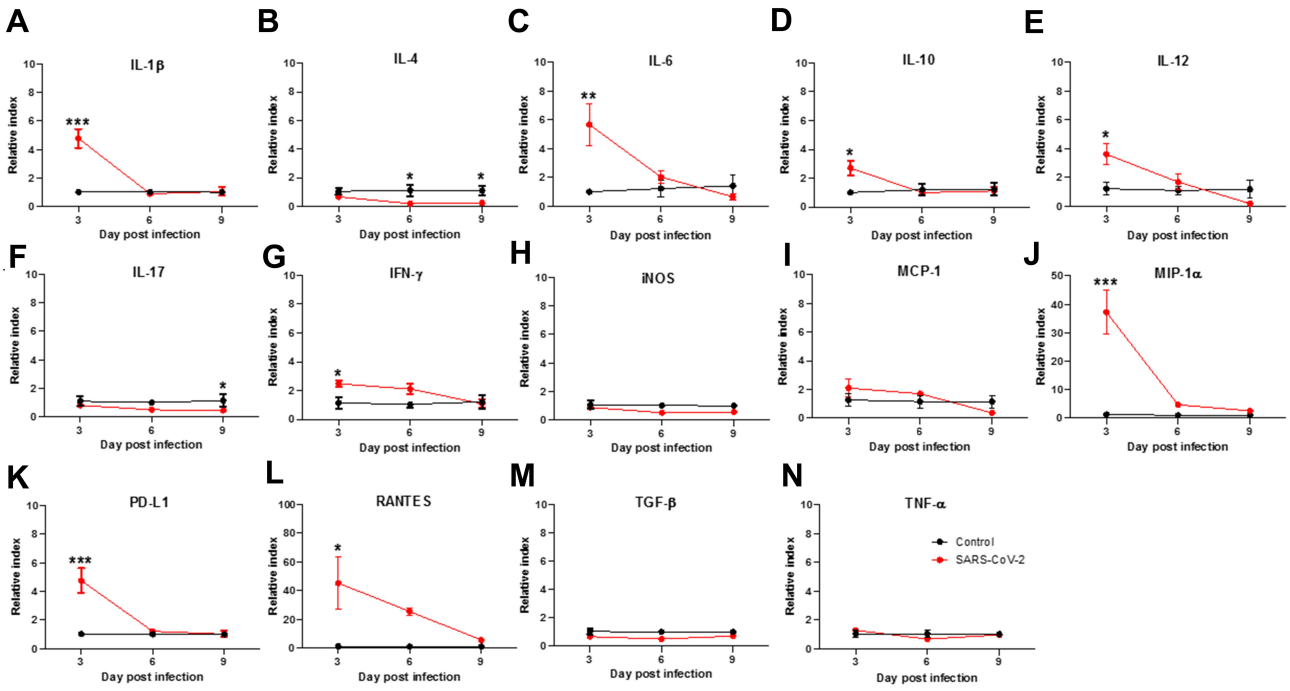

Figure 7 Cytokine expression in lungs of SARS-CoV-2-infected hamsters on days 3, 6, and 9 post-infection. Hamsters were infected with 5×10^5 $TCID_{50}$ of SARS-CoV-2 (n=5 for SARS-CoV-2, and n=3 for non-infected control). On days 3, 6, and 9 post-infection, the hamsters were sacrificed, lung RNA was extracted, and cytokine gene expression profiles were determined by using qPCR. Relative index is presented as $2^{-\Delta\Delta CT}$ and the mean ± SEM of the numeric values in each SARS-CoV-2 group is also presented below at 3, 6, and 9 d.p.i., respectively. (**A**) IL-1β (4.787±0.592, 0.892±0.159, 1.054±0.270), (**B**) IL-4 (0.665±0.157, 0.190±0.043, 0.238±0.082), (**C**) IL-6 (5.682 ±1.304, 2.038±0.368, 0.666±0.198), (**D**) IL-10 (2.701±0.466, 1.004±0.143, 1.112±0.251), (**E**) IL-12 (3.610±0.653, 1.684±0.499, 0.198±0.024), (**F**) IL-17 (0.804±0.087, 0.493 ±0.0455, 0.456±0.0792), (**G**) IFN-γ (2.479±0.209, 2.106±0.328, 1.094±0.242), (**H**) iNOS (0.883±0.128, 0.513±0.024, 0.560±0.054), (**I**) MCP-1 (2.097±0.543, 1.696±0.171, 0.362±0.049), (**J**) MIP-1α (37.216±6.960, 4.745±0.496, 2.589±0.409), (**K**) PD-L1 (4.754±0.775, 1.221±0.168, 1.025±0.201), (**L**) RANTES (45.247±16.554, 25.458±2.261, 5.574±0.834, (**M**) TGF-β (0.672±0.073, 0.507±0.0231, 0.716±0.1228), (**N**) TNF-α (1.288±0.1220, 0.68±0.0517, 0.968±0.1251). Differences among groups were determined using two-way ANOVA with a Bonferroni post hoc test in panels (**A–N**) (*P < 0.05; **P < 0.01; ***P < 0.001), no significance among groups is not shown.

macrophage inflammatory protein 1α (MIP-1α, also called CCL3, Figure 7J), and RANTES (regulated on activation, normal T cell expressed and secreted, also called CCL5, Figure 7L), but not IL-4 (Figure 7B), IL-10 (Figure 7D), IL-17 (Figure 7F), IFN-γ (Figure 7G), iNOS (Figure 7H), MCP-1 (Figure 7I), and TGF-β (Figure 7M). The levels of IL-1β (Figure 7A, relative index = 4.787 ± 0.592, ***P<0.001), IL-6 (Figure 7C, relative index = 5.682 ± 1.304, **P<0.01), IL-12 (Figure 7E, relative index = 3.61 ± 0.653, *P<0.05), IFN-γ (Figure 7G, relative index = 2.479 ± 0.209, *P<0.05), MIP-1α (Figure 7J, relative index = 37.216 ± 6.961, ***P<0.001) and RANTES (Figure 7L, relative index =45.25 ± 16.554, *P<0.05) were particularly elevated at 3 d.p.i. However, the levels of IL-17 (Figure 7F, relative index = 0.804 ± 0.087), IFN-γ, monocyte chemoattractant protein (MCP-1, also called CCL2, Figure 7I, relative index = 2.097 ± 0.543), and TNF-α (Figure 7N, relative index = 1.288 ± 0.122) at 3 d.p.i. were lower than expected for general viral infections, and especially in so-called hypercytokinemia in severe COVID-19 patients.[17,18] Therefore, we also measured the expression levels of some immune suppressor genes to determine whether they may be inhibiting cytokine production. As shown in Figure 7, both IL-10 (Figure 7D, relative index = 1.606 ± 0.548, *P<0.05) and programmed death-ligand 1 (PD-L1) (Figure 7K, relative index = 4.754 ± 0.775, ***P<0.001) were significantly elevated at 3 d.p.i. This result suggests that SARS-CoV-2 may induce the expression of some immune suppressors to attenuate immune responses. As a reference, the results of qPCR of cytokine genes in heart (Supplementary Figure 2) and kidney (Supplementary Figure 3), where no inflammatory signs were evident, showed normal levels of expression.

Increased Amylase, Lipase Level and GOT/GPT Ratio in the Blood of SARS-CoV-2-Infected Hamsters

To dissect clinically relevant changes over the course of SARS-CoV-2 infection in hamsters, we examined multiple chemistry parameters in plasma. The levels of amylase and lipase, which reflect damage to the pancreas and acute pancreatitis, showed moderate increases with time post

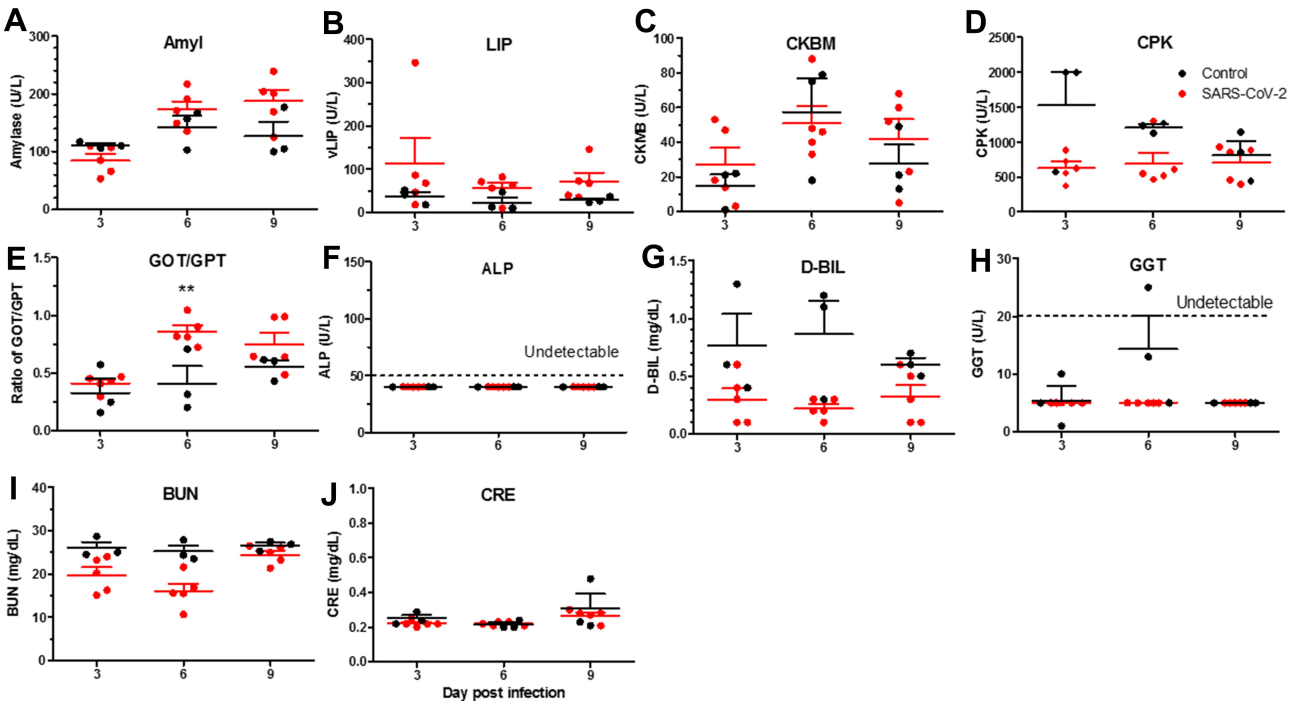

Figure 8 Blood biological and chemistry parameters in SARS-CoV-2-infected hamsters on days 3, 6, and 9 post-infection. Hamsters were infected with 5×10^5 $TCID_{50}$ of SARS-CoV-2 (n=5 for SARS-CoV-2, and n=3 for non-infected control). On days 3, 6, and 9 post-infection, plasma was collected and stored at −80°C until use. Multiple biological and chemistry parameters were analyzed with Fuji Dri-Chem slides on a Fujifilm Dri-Chem 4000 analyzer. (**A**) Amylase (Amyl). (**B**) Lipase (LIP). (**C**) Creatine phosphokinase isozyme KB (CKMB). (**D**) Creatine phosphokinase (CPK). (**E**) Ratio of glutamic oxalacetic transaminase/glutamic pyruvic transaminase (GOT/GPT). (**F**) Alkaline phosphatase (ALP). (**G**) Direct Bilirubin (D-BIL). (**H**) γ-Glutamyltransferase (GGT). (**I**) Urea nitrogen (BUN). (**J**) Creatinine (CRE). Differences among groups were determined using two-way ANOVA with a Bonferroni post hoc test in panels (**A–J**) (**$P < 0.01$), no significance among groups is not shown.

infection, compared to the non-infected control (Figure 8A and B); however, the differences are not statistically significant. Similarly, we detected no differences in the levels of CKMB and CPK, markers of acute hepatitis (Figure 8C and D). The GOT/GPT (AST/ALT) ratio is a measure of liver damage and hepatotoxicity. At 3 d.p.i., the ratio was nearly the same between the control and SARS-CoV-2 groups (Figure 8E); at 6 d.p.i. it increased significantly in the SARS-CoV-2 group, and then decreased at 9 d.p.i. (Figure 8E). The levels of ALP, BUN, and GGT, which are indicators of hepatitis and biliary obstruction, were not significantly changed (Figure 8F-H). BUN and CRE, markers of kidney damage and acute renal disease, showed no significant difference between the SARS-CoV-2 and control groups (Figure 8I and J). Also, we consigned hamster plasma samples to the Inflammation Core Facility of the Institute of Biomedical Sciences (Academia Sinica, Taiwan) to perform the Multi-Plex immune assay to determine whether cytokines expressed in the lung are also expressed in the plasma, including IL-1β, IL-6, IL-12, IL-17A, IFN-γ, and TNF-α. We found that the expression of IL-1β (Supplementary Figure 4A), TNF-α (Supplementary Figure 4D), IFN-γ (Supplementary Figure 4E), and IL-17A (Supplementary Figure 4F) was higher in plasma of SARS-CoV-2-infected hamsters compared to controls. The levels of IL-6 and IL-12 were not significantly different between these two groups (Supplementary Figure 4B and C).

Discussion

The clinical and physiological signs we observed in Syrian hamsters infected by beta coronavirus/SARS-CoV-2/Taiwan 2020-004 are consistent with those recently reported for this rodent species.[4,7–11] Body weight loss, viral load, and recovery over the 14-day study period appeared to be independent of viral dose for the three doses we tested. Viral load was highest at 3 d.p.i. (compared to 6 and 9 d.p.i), as were viral RNA and viral nucleoprotein levels. Severe inflammation and pneumonia appeared at 6 d.p.i., coinciding with the lowest body weight. Subsequently, weight loss and other signs of illness began to improve daily until day 14. Thus, the infectious cycle in the hamster is a good proxy for that of humans. PAS staining revealed phagocytosis of cell debris and excess secretion of mucus at 3 and 14 d.p.i. This

mirrors the condition of excess mucus secretion in COVID-19 patients. Moreover, cell infiltration still appeared in the lungs in the absence of detectable virus or nucleoprotein expression at 14 d.p.i., suggesting that residual viral debris or cellular debris from damaged cells may continue to trigger an inflammatory response. The main target of SARS-CoV-2 is the lungs, but small amounts of virus also appeared in liver, pancreas, heart, kidney, PBMC, and even bone marrow; however, no visible damage appeared in these organs and tissues except liver.

The liver and pancreas findings are interesting. Although no inflammation and cell infiltration was observed in these organs of SARS-CoV-2-infected hamsters, structural abnormalities and large vacuoles were detected in the liver. Based on IHC nucleoprotein staining, viral protein expression coincided with the location of the large vacuoles in hepatocytes, indicating that virus did replicate in the liver. However, it is perplexing that this invasion by SARS-CoV-2 of the liver did not elicit an obvious immune response. The interaction of SARS-CoV-2 and hepatocytes is worth further study. Similar hepatic structural abnormalities and large vacuoles were observed in a patient with severe COVID-19,[16] nevertheless, cirrhotic nodules with thick fibrosis, mild sinusoidal dilatation, focal hepatic necrosis in the periportal zone, and focal centrilobular necrosis which occurred in some severe cases were not found in our hamsters.[19] COVID-19-associated acute pancreatitis has been reported in 17–18% of clinical cases;[20,21] however, there is no evidence to suggest that the viral attack caused the pancreatitis or other pancreatic injury. The pancreases of all infected hamsters in our study had detectable viral loads of approximately 10^4 $TCID_{50}$ at 3 and 6 d.p.i., but no immune-cell infiltration or nucleoprotein expression was found. Although virus apparently did replicate in the pancreas, the absence of both nucleoprotein and an immune response is surprising, but might be explained if pancreatic enzymes had digested many of the viral proteins. The different pathological findings in hamster (asymptomatic and mild cases) versus human (ie, severe cases whose organs were examined after death, but not asymptomatic or mild ones) may be a reflection of the severity and the outcome of COVID-19 cases and their underlying diseases like hepatitis and diabetes.

In the early stage of SARS-CoV-2 infection, host cells turn on their antiviral factors. Some clinical cases also showed that cytokine storms caused by SARS-CoV-2 can lead to patient death.[17,18] At 3 d.p.i., we detected high levels of expression of IL-1β, IL-6, IL-12, MIP-1α, and RANTES, but not TNF-α (the key driver of inflammation, especially in virus infection), MCP-1, iNOS, and IL-17. We do not have data for IFN-α and IFN-β for hamsters; however, some of our qPCR results of cytokine expression in SARS-CoV-2-infected hamster lung (such as IL-6, IL-10, and TNF-α) mirror the cytokine profile detected in plasma and blood of clinical COVID-19 patients.[18,22] Our H&E staining revealed extensive cell infiltration, diffuse alveolar damage, acute bronchopneumonia, fluid exudate, and small areas of vasculitis in SARS-CoV-2-infected hamster lung. However, the cytokine expression profile did not fully match the H&E pathological findings at 3 and 6 d.p.i. Therefore, we wondered whether some immune suppressor genes might have been activated by the virus to inhibit production of certain important cytokines. Interestingly, our qPCR results indicated significant expression of IL-10 (Figure 7D) and PD-L1 (Figure 7K). IL-10 (cytokine synthesis inhibitory factor, CSIF) is an anti-inflammatory cytokine, primarily produced by monocytes. PD-L1 is an immune checkpoint factor which plays a major role in suppressing the adaptive immune system. High levels of expression of IL-10 and PD-L1 inhibit immune responses and may be linked to the lymphopenia, macrophage dysfunction and delayed production of IFN-γ observed in COVID-19 patients.[23,24] Unfortunately, we do not have other tools (such as IHC, ELISA, FACS, or protein detection) to confirm these data, owing to current limitations of detection methods in the hamster model. Human and mouse models have the most resources, availability, and detection tools (from DNA to protein), including state-of-the-art single-cell RNA sequencing, and this is a current limitation of other model species, including hamsters. The mechanism of immune suppression by SARS-CoV-2 is worth further study.

Although most people infected with SARS-CoV-2 are asymptomatic or have mild disease, it is still vitally important to discover biomarkers and indicators of COVID-19 to aid in diagnosis and prevention. Biological and chemistry parameters in plasma may be a good option. In plasma of SARS-CoV-2-infected hamsters, we detected increased amylase (Figure 8A), lipase (Figure 8B), and ratio of GOT/GPT (Figure 8E, particularly GOT/GPT), and viral RNA in the liver (Figure 3C) and pancreas (Figure 3D) was also detected, suggesting that some tissue injury may be induced by virus invasion to cause tissue damage directly. Elevated GOT, GPT, and bilirubin of COVID-19

patients have been reported.[25–28] Laboratory findings suggestive of pancreatic injury have been reported in 8.5–17.3% of COVID-19 patients, and the raised lipase rate was between 2.8% and 16.8%.[20,29–31] The measured increases in amylase and lipase were low and the results are similar to those we observed in hamsters (Figure 8A and B). Clinical observations of COVID-19 patients with underlying diseases, such as hepatitis, diabetes, cardiovascular and renal diseases and others, showed associations of these diseases with severity of COVID-19.[32,33] Although COVID-19-associated liver and pancreas injury is mild, it may significantly impact the outcome and disease course. Indeed, hepatic and pancreatic dysfunction are highly correlated with the severity of COVID-19, contributing to increased ICU admission and intubation and potentially to multisystem manifestations.[31] Some of these parameters (or combinations of them) may have potential as optimal tools for clinical analysis. However, further study and larger samples sizes are necessary to evaluate this potential.

Acknowledgments

We thank all members who risked exposure to SARS-CoV-2 to complete the animal study. We thank the Core Instrument Center of Pathology and the Laboratory Animal Center of the National Health Research Institutes (the animal facility of ABSL3, AAALAC, NHRI) for technical assistance and consultation. We thank the Inflammation Core Facility, Institute of Biomedical Sciences (Academia Sinica, Taiwan) for conducting the Multi-Plex immunoassay. We also thank CW Hsu, WC Lo, JR Chang, YT Chiu, Dr. TT Tzeng, and Dr. JJ Lin for experimental and administration assistance.

Disclosure

The authors report no conflicts of interest in this work.

References

1. Zhu N, Zhang D, Wang W, et al. A novel coronavirus from patients with pneumonia in China, 2019. *New Engl J Med*. 2020;382(8):727–733. doi:10.1056/NEJMoa2001017
2. WHO. *Coronavirus Disease (COVID-19) Pandemic*; 2020.
3. Li W, Moore MJ, Vasilieva N, et al. Angiotensin-converting enzyme 2 is a functional receptor for the SARS coronavirus. *Nature*. 2003;426(6965):450–454. doi:10.1038/nature02145
4. Chan JF-W, Zhang AJ, Yuan S, et al. Simulation of the clinical and pathological manifestations of Coronavirus Disease 2019 (COVID-19) in golden Syrian hamster model: implications for disease pathogenesis and transmissibility. *Clin Infect Dis*. 2020:ciaa325. doi:10.1093/cid/ciaa325.
5. Jia HP, Look DC, Shi L, et al. ACE2 receptor expression and severe acute respiratory syndrome coronavirus infection depend on differentiation of human airway epithelia. *J Virol*. 2005;79(23):14614–14621. doi:10.1128/JVI.79.23.14614-14621.2005
6. Roberts A, Vogel L, Guarner J, et al. Severe acute respiratory syndrome coronavirus infection of golden Syrian hamsters. *J Virol*. 2005;79(1):503–511. doi:10.1128/JVI.79.1.503-511.2005
7. Sia SF, Yan L-M, Chin AWH, et al. Pathogenesis and transmission of SARS-CoV-2 in golden hamsters. *Nature*. 2020;583(7818):834–838. doi:10.1038/s41586-020-2342-5
8. Warner BM, Safronetz D, Kobinger GP. Syrian hamsters as a small animal model for emerging infectious diseases: advances in immunologic methods. *Adv Exp Med Biol*. 2017;972:87–101. doi:10.1007/5584_2016_135
9. Brocato RL, Principe LM, Kim RK, et al. Disruption of adaptive immunity enhances disease in SARS-CoV-2 infected Syrian hamsters. *bioRxiv*. 2020. doi:10.1101/2020.06.19.161612
10. Lee AC-Y, Zhang AJ, Chan JF-W, et al. Oral SARS-CoV-2 inoculation establishes subclinical respiratory infection with virus shedding in golden Syrian hamsters. *Cell Rep Med*. 2020:100121. doi:10.1016/j.xcrm.2020.100121.
11. Monchatre-Leroy E, Lesellier S, Wasniewski M, et al. Hamster and ferret experimental infection with intranasal low dose of a single strain of SARS-CoV-2. *bioRxiv*. 2020. doi:10.1101/2020.09.24.311977
12. Bao L, Deng W, Huang B, et al. The pathogenicity of SARS-CoV-2 in hACE2 transgenic mice. *Nature*. 2020;583(7818):830–833. doi:10.1038/s41586-020-2312-y
13. Winkler ES, Bailey AL, Kafai NM, et al. SARS-CoV-2 infection of human ACE2-transgenic mice causes severe lung inflammation and impaired function. *Nat Immunol*. 2020. doi:10.1038/s41590-020-0778-2
14. Guan W-J, Ni Z-Y, Hu Y, et al. Clinical characteristics of coronavirus disease 2019 in China. *New Engl J Med*. 2020;382(18):1708–1720. doi:10.1056/NEJMoa2002032
15. Diao B, Wang C, Tan Y, et al. Reduction and functional exhaustion of T cells in patients with coronavirus disease 2019 (COVID-19). *Front Immunol*. 2020;11:827. doi:10.3389/fimmu.2020.00827
16. Xu Z, Shi L, Wang Y, et al. Pathological findings of COVID-19 associated with acute respiratory distress syndrome. *Lancet Respir Med*. 2020. doi:10.1016/s2213-2600(20)30076-x
17. Mehta P, McAuley DF, Brown M, Sanchez E, Tattersall RS, Manson JJ. COVID-19: consider cytokine storm syndromes and immunosuppression. *Lancet*. 2020;395(10229):1033–1034. doi:10.1016/s0140-6736(20)30628-0
18. Pedersen SF, Ho Y-C. SARS-CoV-2: a storm is raging. *J Clin Invest*. 2020;130(5):2202–2205. doi:10.1172/JCI137647
19. Tian S, Xiong Y, Liu H, et al. Pathological study of the 2019 novel coronavirus disease (COVID-19) through postmortem core biopsies. *Mod Pathol*. 2020;33(6):1007–1014. doi:10.1038/s41379-020-0536-x
20. Wang F, Wang H, Fan J, Zhang Y, Wang H, Zhao Q. Pancreatic injury patterns in patients with coronavirus disease 19 pneumonia. *Gastroenterology*. 2020;159(1):367–370. doi:10.1053/j.gastro.2020.03.055
21. Liu F, Long X, Zhang B, Zhang W, Chen X, Zhang Z. ACE2 expression in pancreas may cause pancreatic damage after SARS-CoV-2 infection. *Clin Gastroenterol Hepatol*. 2020;18(9):2128–2130.e2122. doi:10.1016/j.cgh.2020.04.040
22. Hadjadj J, Yatim N, Barnabei L, et al. Impaired type I interferon activity and inflammatory responses in severe COVID-19 patients. *Science*. 2020;369(6504):718. doi:10.1126/science.abc6027
23. Zhou Z, Ren L, Zhang L, et al. Heightened innate immune responses in the respiratory tract of COVID-19 patients. *Cell Host Microbe*. 2020;27(6):883–890.e882. doi:10.1016/j.chom.2020.04.017
24. Blanco-Melo D, Nilsson-Payant BE, Liu WC, et al. Imbalanced host response to SARS-CoV-2 drives development of COVID-19. *Cell*. 2020;181(5):1036–1045.e1039. doi:10.1016/j.cell.2020.04.026

25. Kulkarni AV, Kumar P, Tevethia HV, et al. Systematic review with meta-analysis: liver manifestations and outcomes in COVID-19. *Aliment Pharmacol Ther*. 2020;52(4):584–599. doi:10.1111/apt.15916
26. Yadav DK, Singh A, Zhang Q, et al. Involvement of liver in COVID-19: systematic review and meta-analysis. *Gut*. 2021;70 (4):807. doi:10.1136/gutjnl-2020-322072
27. Kumar-M P, Mishra S, Jha DK, et al. Coronavirus disease (COVID-19) and the liver: a comprehensive systematic review and meta-analysis. *Hepatol Int*. 2020;14(5):711–722. doi:10.1007/s12072-020-10071-9
28. Paliogiannis P, Zinellu A. Bilirubin levels in patients with mild and severe Covid-19: a pooled analysis. *Liver Int*. 2020;40(7):1787–1788. doi:10.1111/liv.14477
29. Bruno G, Fabrizio C, Santoro CR, Buccoliero GB. Pancreatic injury in the course of coronavirus disease 2019: a not-so-rare occurrence. *J Med Virol*. 2021;93(1):74–75. doi:10.1002/jmv.26134
30. McNabb-Baltar J, Jin DX, Grover AS, et al. Lipase elevation in patients with COVID-19. *Am J Gastroenterol*. 2020;115(8):12 86–1288. doi:10.14309/ajg.0000000000000732
31. Barlass U, Wiliams B, Dhana K, et al. Marked elevation of lipase in COVID-19 disease: a Cohort Study. *Clin Transl Gastroenterol*. 2020;11(7):e00215–e00215. doi:10.14309/ctg.0000000000000215
32. Wang Y, Liu S, Liu H, et al. SARS-CoV-2 infection of the liver directly contributes to hepatic impairment in patients with COVID-19. *J Hepatol*. 2020;73(4):807–816. doi:10.1016/j.jhep.20 20.05.002
33. Puelles VG, Lütgehetmann M, Lindenmeyer MT, et al. Multiorgan and renal tropism of SARS-CoV-2. *N Engl J Med*. 2020;383 (6):590–592. doi:10.1056/NEJMc2011400